Damage intitiation and growth in metals. Comparison between modelling and tomography experiments

E Maire, Cyril Bordreuil, Laurent Babout, Jean-Claude Boyer

Damage initiation and growth in metals. Comparison between modelling and tomography experiments

Eric Maire[a,*], Cyril Bordreuil[b,1], Laurent Babout[a,2], Jean-Claude Boyer[b]

[a]*G.E.M.P.P.M, INSA de Lyon, 20, avenue Albert Einstein, 69621 Villeurbanne cedex, UMR CNRS 5510, France*
[b]*L.A.M.C.O.S, INSA de Lyon, 20, avenue Albert Einstein, 69621 Villeurbanne cedex, France*

Damage in heterogeneous model materials was measured using high-resolution X-ray absorption tomography. The material consisted of an aluminium matrix containing 1% and 4% of spherical ceramic particles acting as nucleation sites for an interface decohesion mechanism of damage. The damage initiation stage was quantified using the global population of particles in the 4% material. A strain path change experiment was then applied to the 1% material. The sample was first deformed in tension in order to create elongated cavities and then compressed at 45° to rotate and close these cavities. The results of a model based on the Rice and Tracey approach accounting for the presence of particles inside the cavities and calculating their rotation with assuming a linear hardening plastic behaviour of the matrix were compared with the observations. The model was modified to account for the damage

*Corresponding author.
E-mail addresses: eric.maire@insa-lyon.fr (E. Maire), cyril_bordreuil@yahoo.fr (C. Bordreuil).
[1]Now at LMGC-IUT de Nimes, dpt GMP, 8, rue Jules Raimu/30907 Nimes.
[2]Now at the University of Manchester, School of Materials. Materials Science Center M1 7HS Manchester, UK.

initiation phase. It was shown to give a good global prediction of the void volume fraction provided that the physical, mechanical and morphological information are corresponding in the experimental and the model cases. The cavity rotation experiment was also shown to compare well with the calculation although only one cavity was sufficiently opened after compression to allow the comparison.

Keywords: Damage; Growth; Inclusion; Metal; Tomography

1. Introduction

From a physical point of view, damage, defined as the appearance of new surfaces in a material, can be decomposed into three stages: initiation, growth and then coalescence. It has been shown (Sarkar et al., 2001) that damage initiates preferentially at special sites, such as heterogeneous inclusions. Different initiation mechanisms have been observed: inclusion rupture (Llorca et al., 1993), inclusion/matrix decohesion (Dierickx et al., 1996) or matrix cracking around the inclusions in the case of fatigue of metals.

Modelling damage evolution in material science is of great importance to predict the rupture during different kinds of loadings. Many studies have for instance dealt with the ductile fracture of metals during a tensile experiment (Manoharan and Lewandowski, 1989; Humphreys, 1989; Poza and Llorca, 1996; Verhaege et al., 1997). Another important field is the more complicated rupture prediction during forming processes of metals at high (hot rolling, forging) (Semiatin et al., 1998) or low (cold rolling, stamping) temperatures (Tvergaard and Needleman, 1984).

Many theoretical studies have been carried out from a mechanical point of view, especially devoted to the initiation and the growth stages of the process. Several damage initiation criteria have been developed (Beremin, 1981). The growth stage is the most extensively studied from a modelling point of view. These damage growth models can be divided into two categories: the uncoupled and the coupled approaches. The uncoupled approaches based on the work by Rice and Tracey (denoted RT henceforth) (Rice and Tracey, 1969) only predict the evolution of the size of the voids. Based on the variational principle of RT, Budiansky et al. (1982) studied the effect of viscosity on the growth of the rate of expansion. Lee and Mear (1992) modified the growth model for the axisymmetric ellipsoidal shape. It was shown by Huang (1991) that the initial RT solution underestimates quite strongly the dilatation rate so should not be used in its initial form. The coupled approaches evaluate the modification of the global behaviour of the material according to the new volume fraction of voids. Gurson (1977) proposed a macroscopic potential for a spherical void based on a homogenization process. Other contributions introduced different considerations. For example, Gologanu et al. (1994) integrated the law proposed by Lee and Mear (1992) and Benzerga and Besson (2001) introduced the influence of matrix orthotropy. In a more recent contribution Pardoen and

Hutchinson (2000) take into account some features of the microstructure such as the hole spacing.

Despite the interest of the previous studies and their different improvements, none of the existing models satisfy all the physical conditions of the phenomenon. In this field, it is important to compare the results of the predictions of the different modelling approaches with key experiments, in order to identify the actual physical parameters used in the different modelling methods. This comparison is tricky because experimental observation of damage is a complicated problem. Damage can be studied from surface observation during in situ tensile tests but it has been shown recently (Buffière et al., 1999) that the information obtained, although very good qualitatively, can be wrong quantitatively because of surface effects on the stress field. Damage can also be studied by post mortem observation of polished internal surfaces. However the polishing can induce a lot of artificial disturbances and bias the quantitative analysis. X-ray tomography has emerged during the last decade as a new powerful characterization technique to visualize the interior of an opaque sample (Maire et al., 2001). It does not exhibit the drawbacks of more conventional methods but only a few investigations of damage have been attempted so far using this non-destructive imaging method. The damage observation problem mentioned above is not the only obstacle to a good quantitative comparison between models and experiments. The materials generally used for comparison contain inclusions with complicated shapes, whereas the models usually deal with spherical geometry.

The aim of the present paper is to compare, in the case of a model material containing spherical inclusions (Babout et al., 2001, 2004), the predictions of a physically based model (Bordreuil et al., 2004) with the experimental observation and quantification performed using X-ray tomography. The proposed model is based on the RT approach. It has been chosen because it is focused on damage growth around an inclusion within a hardening matrix and it can be used to assess cavity rotation. It is modified in the present study to take into account a delay in the initiation process identified by key experimental observations. For the first time, comparisons between the model and local measurements performed by means of tomography observations are shown in the case of tensile and multiple loading path experiments.

2. Experimental conditions

Two specific experimental tools were used in the present paper in order to improve the comparison between experiments and modelling:

- Void nucleation and void growth were analysed and then quantified using the new high-resolution X-ray tomography technique. Such very local measurement is extremely new in this field of comparison between damage modelling and damage observation.

- Deformation experiments were performed on model materials with a microstructure as close as possible to the modelling hypothesis (low volume fraction of spherical hard inclusions in a ductile matrix).

These tools are described in the following paragraphs together with the cold deformation applied to the samples.

2.1. X-ray microtomography

The experimental part of this study was focused on the use of a three-dimensional (3D) non-destructive technique, the high-resolution X-ray absorption tomography. Disturbance-free information about the microstructure throughout the volume could be obtained. Very detailed descriptions of this technique can be found in Buffière et al. (1999), Maire et al. (2001). For the understanding of the present paper, the important features of this characterization method are briefly summarized here.

Tomography combines the information of a high number of X-ray absorption radiographs of the sample taken with different viewing angles. The technique employs computation i.e. it includes a recalculation step during which the 3D map of the local absorption coefficients in each elementary volume of the sample is retrieved from the set of absorption radiographs. This map gives an indirect image of the microstructure.

In the present study, the samples were scanned using a high-resolution X-ray tomograph located at the ESRF (beam line ID 19) in Grenoble (France) (<http://www.esrf.fr/expfacilities/id19/homepage/id19homepage.html>, 2000). X-ray tomography was performed at a resolution of 0.7 μm. The energy was set to 20 keV. The distance between the sample and the detector was about 7 cm. A set of 1800 projections were taken within 180°. The detector was a CCD camera with 2048 × 2048 sensitive elements coupled with an X-ray sensitive laser screen. The field of view of the detector was about 1.4 mm wide.

2.2. Materials

2.2.1. Choice of the model system

The materials used were composed of a pure aluminium matrix reinforced with two different amounts (1% and 4%) of spherical inclusions. The 4% material was equivalent to the one investigated in Babout et al. (2004) while the one with the lower volume fraction was produced especially for the present study. The matrix was a 99.9% pure aluminium. The unreinforced material was very soft, with a low yield stress (75 MPa) and a very high value of ductility (0.5). The composites were made using powder metallurgy technology (see next section). The size of the initial matrix powder was selected to be lower than 20 μm. The inclusions were a mixture of zirconia (70% in weight) and silica (30% in weight) kindly provided by the SEPR St Gobain company. The commercial name of the product is Zirblast™ (for more information on these particles, see <http://www.zirpro.com>, 2000). It is supplied as nearly spherical beads with a tailored size, which was screened by shifting between

20–60 μm in the present study. This rather large size was chosen because of the 0.7 μm resolution in the reconstructed images obtained by X-ray tomography. The size has also to fulfil the assumptions of the Continuum Mechanics approach (as opposed to the dislocation approach) in order to handle the problem with consistent assumptions.

2.2.2. *Manufacturing process*

The matrix powder and the ZS particles were mixed for 1 h to disperse the reinforcement homogeneously in the matrix. Then, the mixture was hot pressed in vacuum ($P_{\text{vacuum}} = 10^{-3}$ Torr, $T = 450\,^{\circ}\text{C}$, $t = 20$ min, $P = 70$ MPa). The resulting cylinders (40 mm in diameter and 30 mm in length) were then extruded with a pressure close to 250 MPa. The applied extrusion ratio of 16:1 gave an extruded circular bar of 10 mm in diameter. After extrusion, the bar was annealed at a homogenization temperature of 530 °C for 1 h and then quenched in water.

2.3. *Ex situ cold deformation—strain path change*

A small tapered sample was cut from the material reinforced with 1% of inclusions. The microstructure of this material is very close to the modelling hypotheses (low volume fraction) although it contains less particles than the 4% one. As a consequence the number of observed damage active sites is expected to be smaller leading to conclusions likely to be less statistically representative. The

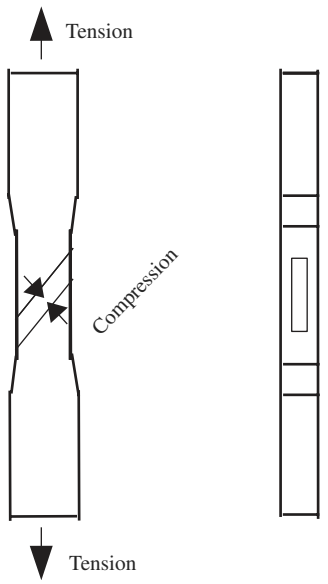

Fig. 1. Sketch of the geometry of the tensile sample used. The subsequent cutting of the compression sample is also shown in the figure.

geometry of the sample is shown in Fig. 1. It was cut from the centre of the bar with its axis parallel to the extrusion direction. The overall length of the sample was 40 mm and its gauge length was 10 mm long with a section of 3×3 mm. A standard load frame with wedge-action grips was firstly used to apply the tensile load at a deformation speed $\dot{\varepsilon}$ of 10^{-3} up to a true strain of 0.5. The goal of this initial straining was the creation of elongated voids in the polar regions of the ceramic beads, such as those observed in Babout et al. (2004). The presence of these voids after the first step was mandatory because one of the aims of the present paper was to study the rotation of these initially created cavities. This first step of the straining was experimentally performed in three strain sub-steps of about 0.16 each. Between each of these steps, the sample was re-annealed at 530 °C for 1 h in order to restore the initial work hardening ability of the material. With this process, the sample could be homogeneously strained up to a very large plastic deformation without necking. After the tensile loading, a compression parallelepipedic sample of $1 \times 1 \times 4$ mm was machined with its long axis oriented at 45° of the extrusion/tension direction (see Fig. 1). The compression sample was cut in the middle of the initial tensile specimen. After tomographic scanning for retrieving the 'tensiled' microstructure, the parallelepipedic sample was compressed at room temperature, with the same deformation rate $\dot{\varepsilon}$ of 10^{-3} but in the direction at 45° from the initial tensile direction (see Fig. 1).

2.4. In situ tensile test

Constant strain rate in situ tensile tests were finally carried out at room temperature on the material reinforced with 4% of inclusions using a specially designed machine for in situ tensile measurements during tomography. The sample geometry and experimental conditions were the same as those described in Babout et al. (2004). On this particular sample, five scans were performed, the first corresponding to the initial undeformed state and the others to increasing strain levels. This experiment was carried out to quantitatively measure the initiation stage of damage in this kind of material. This was performed on the 4% material because it contains four times more particles in the same examined volume than the 1% one.

3. Experimental results

3.1. Qualitative results

The qualitative results of the in situ tensile test were very similar to these presented in Babout et al. (2004). These results will be used more extensively for the quantitative comparison between experiments and modelling in the rest of the paper. We focus in the present section on the qualitative results of the strain path change experiment. The same parallelepipedic sample was observed by tomography before and after the compression at 45° of the two-path deformation process described above. During these two scans, the orthogonal directions of the compression sample

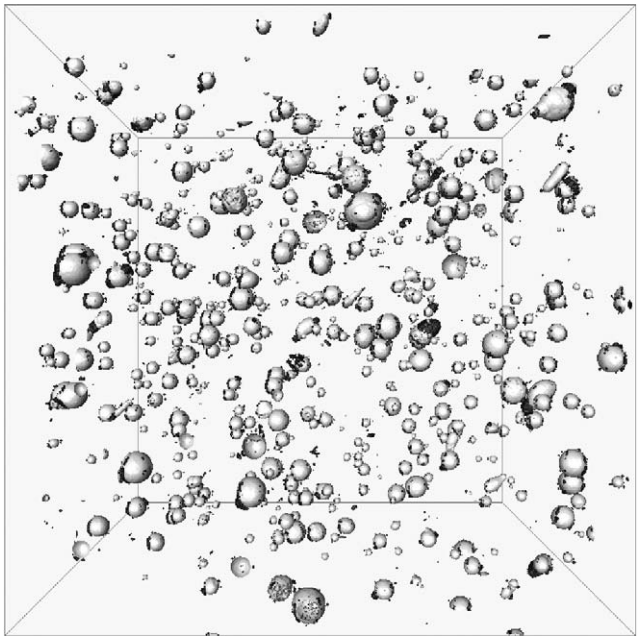

Fig. 2. 3D view of the sample after the tensile loading. The voxels in the aluminium have been removed. The cavities are highlighted in black and the particles in white. The cavities created by the tensile strain path are aligned at 45° with respect to the main direction of the compression sample.

were aligned with the imaging set-up so that, in the reconstructed 3D image, the axes of the porosities created during tension were oriented at 45° with respect to the main directions of the image. Fig. 2 shows a 3D view of the material in the state after tension (i.e. before compression). The 45° direction of the pores after the first loading path is clearly seen in this figure. It is worth noting that cavities have nucleated only for a small fraction of the inclusions and that this nucleation certainly appeared at different tensile strain levels as the values of the main cavity radii are not uniform. This set of results is consistent with the measurements presented in Babout et al. (2004). Fig. 3 shows a comparison of two tomographic slices extracted from the parallelepipedic sample. The image on the left shows the microstructure after the tensile loading. A large void has been created at the polar region of this particle; this cavity is one of the biggest observed in the material strained under tensile stress state. The rupture of the particle observed in this particular case was not representative of the situation in the material which exhibited a majority of decohesions rather than ruptures. It is assumed that this rupture at the opposite pole of the decohesion site does not affect the subsequent modelling validation of the rotation of the cavity performed in a later section. The void is elongated at 45° of the axis of this image i.e. along the tensile axis. The extensive growth of this void seems to indicate that it must have nucleated at the beginning of the tensile path. The image on the right in Fig. 3

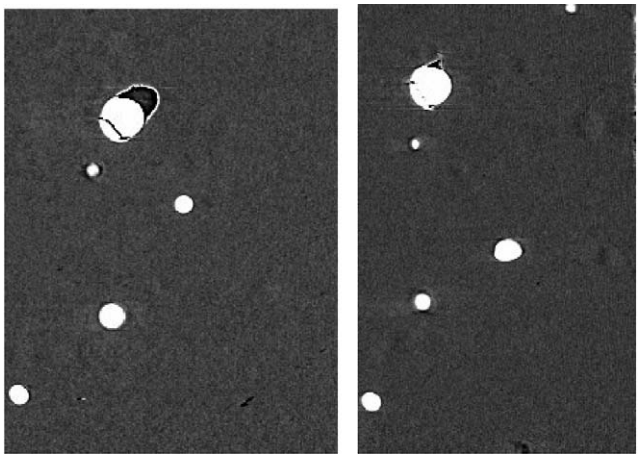

Fig. 3. State of defects after the tensile test followed by the compressive test. The compression axis is horizontal in the figure.

shows the same region for the material after the compression loading (the compression axis is vertical in these two images). These images show clearly that the compression loading induces:

- the rotation of the cavity,
- the reduction of the main radius of the cavity.

It must be noted here that the cavity shown in Fig. 3 is the only one large enough to remain sufficiently opened after compression. As a consequence this image is the only one for which a direct comparison between experimental and a quantitative calculation of the rotation and radii evolution was possible. This will be discussed in a later section.

3.2. Quantitative results

As observed in Fig. 2, the amount of voids in the 1% composite was very small. In order to increase the statistical validity of a quantitative assessment of the damage initiation mechanism in these materials, the data obtained during the in situ tensile test on the composite reinforced with 4% of spheres were used. In this material with a low fraction of inclusions (i.e. still fulfilling the hypothesis of the model) a sufficient amount of damage is observed. From the 3D images, the changes of the fraction of damaged particles, denoted ω in the modelling section, and of the total amount of porosity f were measured as the plastic strain increased. The evolution of both parameters are given in Figs. 4 and 5, respectively. More precisely, Fig. 5 shows the changes of the ratio:

$$\frac{f + f_{p,0}}{f_{p,0}}, \tag{1}$$

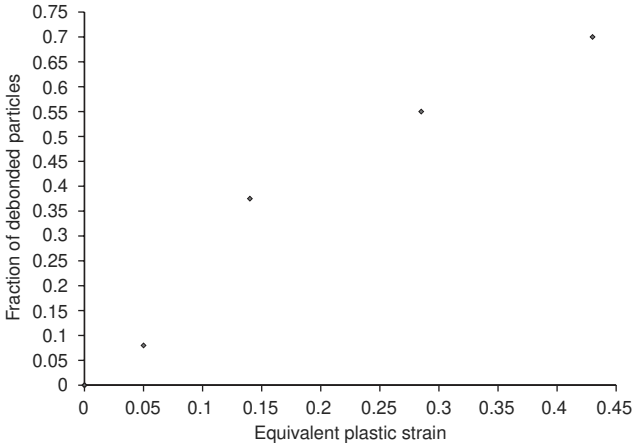

Fig. 4. Evolution of the fraction of damaged particles in the 4% composite material.

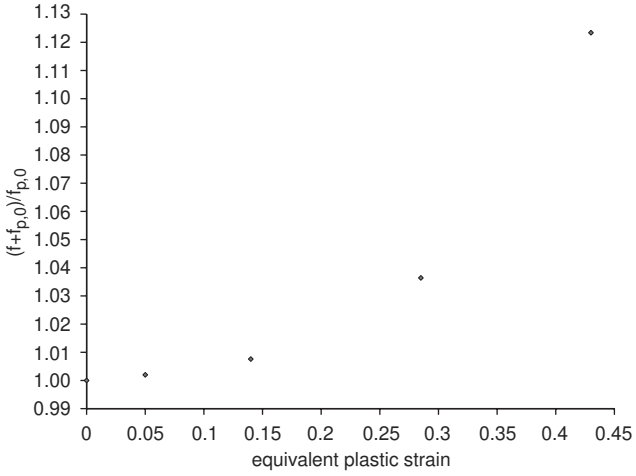

Fig. 5. Evolution of the void volume fraction in the 4% composite material. The total void fraction f is added to the initial fraction of particles $f_{p,0}$ and the sum of the two is rationalized by $f_{p,0}$.

where $f_{p,0}$ is the volume fraction of particles taken here as in many other studies as equal to the initial void volume fraction. Fig. 4 evidences the nucleation threshold which is different from one site another. It can be verified from Fig. 5 that f remains quite small during the tensile test. This experimental result confirms the low volume fraction hypothesis used in the modelling section. This set of experiments is a unique quantification of such a damage process on materials with a well-controlled

microstructure. The quantitative validity of these evolutions cannot be questioned as the 3D technique used to obtain the images is non-destructive and provides indications from the bulk of the material.

4. Damage modelling

This section describes the main features of the existing modelling tools and the improvements performed in the frame of the present study used to compare the results of the model with the experiments described above. The following model has been chosen for its simplicity and the fact that its hypotheses are close to the experimental conditions investigated. It was important, especially for metal forming damage modelling, to choose a model accounting for the presence of a particle, for the plastic hardening of the matrix and dealing with the rotation of cavities as well. This model had to be extended in the present study to account for an initiation stage in the damage process. The initial RT model (Rice and Tracey, 1969) dealt with the growth of a spherical void inside an infinite matrix. This is the starting point of the model used here. One will notice later that because of the implementation of plastic hardening, the initial RT solution was indeed not used in its initial formulation in the present approach. We had to identify the void growth parameters according to comparisons with Finite element calculations. In the following, we only refer to the standard RT formulation for describing simply the way the problem is tackled but one should bear in mind that we do not use its simple form in the comparison calculation.

4.1. Consideration of the presence of a hard inclusion inside a growing void

One of the key issues of the proposed void growth model is the presence of an inclusion in the matrix material. Many authors (Sarkar et al., 2001; Manoharan and Lewandowski, 1989), reported that damage is associated with the presence of hard inclusions in industrial alloys. This presence of a particle has to be accounted for in a physically based mechanical model. Note that the RT model, as the Gurson model and most of their modified extensions, consider empty voids without particle. The implementation of the model considering the presence of an inclusion was discussed in Bordreuil et al. (2004). In short, the radii's defect evolution is given by

$$\dot{r}_i = \left(\frac{5}{3}n_{ii} + \frac{1}{2}\sinh\left(\frac{3}{2}\frac{\sigma_m}{\sigma_0}\right)\right)\bar{D}_{\mathrm{eq}}\bar{r}, \tag{2}$$

where $\bar{r}$ is the mean value given by

$$\bar{r} = (r_1 r_2 r_3)^{1/3}, \tag{3}$$

where σ_m is the mean stress, σ_0 is the yield stress of the matrix, $n_{ii} = \frac{3}{2}\frac{\sigma_{ii}^{\mathrm{D}}}{\sigma_0}$ is the normal to the elastic domain (the upper script D denoted the deviatoric part of the Cauchy stress tensor) and $\bar{D}_{\mathrm{eq}}$ is the equivalent plastic strain rate at infinity. In the proposed model, the coefficient of the sinh, which is equal to 0.558 in the original

RT expression and which was shown by Huang (1991) to be too small, was replaced for sake of simplicity by $\frac{1}{2}$.

The original RT model is devoted to spherical void growth inside an infinite matrix. Under plastic straining, the spherical void elongates and becomes ellipsoidal and the original RT model is no longer valid. Lee and Mear (1992) calculated a displacement field around an axisymmetric void in order to consider the actual shape of the deformed void. In the sequel, the model proposed by Thomason (1988) and based on a slight modification of the original RT model was preferred to account for the effect of the shape change. This effect is introduced via the calculation of the mean radius of the cavity. Some computations, see Bordreuil et al. (2003), showed that this proposal is in good agreement with 3D finite element models of a cell with one spherical void up to 0.5 of equivalent plastic strain.

In the case of a purely dilatational loading, this relation gives an estimation of the void growth rate. Again, Huang's calculations have shown that this solution is not strictly valid but we will use it as a first approximation. The stress state during a tensile test or during forming processes is never purely dilatational. For a low triaxiality ratio loading path, the macroscopic applied plastic strain field can either tend to separate the particle from the matrix (e.g. the strain heterogeneity in the longitudinal direction in a tensile test) or tend to force the contact between the matrix and the inclusion (e.g. because of Poisson's effect in the transverse direction in a tensile test). So, an interaction exists between the matrix and the second phase particle in the area of damaging sites. The more appropriate way to account for the presence of the particle is to redo the RT minimization procedure forcing the radial evolution of the cavity to be equal to zero. A second solution is to use the simple RT framework with no particle while constraining the contact condition in the following way according to what has been done in Bordreuil et al. (2003):

$$\dot{r}_i = 0 \quad \text{if } (\dot{r}_i < 0 \text{ and } r_i = r_{\text{inc}}), \tag{4}$$

where r_{inc} is the radius of the spherical inclusion.

Obviously, the first solution (RT minimization with particle) is closer to reality but the second solution (RT without particle but with constrained evolution of the radii) gives a reasonable estimation for low triaxiality ratios as this has been shown in Bordreuil et al. (2004). It was also shown in Bordreuil et al. (2003) that these two solutions compare quite well with finite element simulations. It was for instance calculated that for a triaxiality ratio smaller than 1, the error in the calculation of the volume fraction of pores remains below 10% up to an applied plastic strain of 1. Again, as will be shown in the following paragraph, both approaches were not used in our final calculations because of the way we have accounted for hardening of the matrix.

4.2. Plastic hardening of the matrix

In some growth models described above, the matrix material is assumed to be elastic perfectly plastic, whereas actual material can exhibit a strain hardening behaviour. It was emphasized by Budiansky et al. (1982) that the rate of growth

decreases with the hardening exponent of the matrix material, so a faster growth is predicted for a rigid plastic matrix. Some authors consider the hardening phenomenon in the frame of a coupled analysis. For instance, Leblond et al. (1995) proposed a modified version of the Gurson potential to take strain hardening into account. In the present work, because small void volume fraction is concerned, the original RT model was used but in a form modified to account for plastic hardening introduced in the following way (see also (Bordreuil et al., 2003)). When the RT model is used under an incremental formulation, it is possible to introduce the influence of the hardening of the matrix ($\sigma_y = \sigma_0 + K\bar{\varepsilon}^{\mathrm{p}}$, where $\bar{\varepsilon}^{\mathrm{p}}$ is the equivalent plastic strain). As the required Lambert function is not easy to use under its analytical expression, a numerical description of this function was chosen. For this purpose, Eq. (2) is transformed into

$$\dot{r}_i = \left(An_{ii} + B\frac{\sigma_m}{\sigma_0} \right) \bar{D}_{\mathrm{eq}} \bar{r}, \tag{5}$$

where A and B are numerical constants identified by minimization of the RT principle for linear hardening (Bordreuil, 2002). These constants are functions of the factor K/σ_0. This law can be used for any complex hardening behaviour described with piecewise linear functions in a first approximation.

In order to fit the stress–strain curve of the pure aluminium, the strain hardening part was simply described with three linear functions, the coefficients (yield stress σ_0 and hardening coefficient K) and the strain range of which are given in Table 1. Note that the last part of the plastic curve is assumed to be perfectly plastic. The coefficients A and B for these three parts of the plastic strain–stress curve of this material are also given in Table 1 (the last part is characterized by RT coefficients).

The value of B can appear to be surprisingly low especially for the first part of the behaviour ($B = 0.02$). This is simply due to the very high hardening coefficient which had to be used to fit the beginning of the hardening of the material used in the experimental part of this study. The results of our analytical treatment of the hardening of the material have again been shown to compare well with 3D FE calculations.

Table 1
Values of the parameters chosen to fit the experimental hardening behaviour of the matrix material

	Strain domain	σ_0	K	A	B
First part	0–0.05	70	600	1.3	0.02
Second part	0.05–0.2	100	10	1.4	0.3
Third part	0.2–∞	115	0	RT	RT

The coefficients A and B used in Eq. (5) for the linearization of the plastic behaviour of the experimental matrix material hardening are also tabulated. The last part, with no hardening, is treated in the RT framework.

4.3. Orientation changes

The previous model based on Eq. (2) is well suited for the proportional loading path because the created void is assumed to grow in the loading direction. Actually, bulk metal forming involves multi-step processes, where the nucleated voids are no longer aligned in the new directions of loading. The growth process can be greatly modified by these orientation changes.

Only a few damage models considering orientation effects can be found in the literature (Bilby and Kolbuszewski, 1977; Fleck and Hutchinson, 1986; Kailasam and Ponte-Castañeda, 1998). In the present work, a void growth model including orientation changes was developed and added to the previous approach (Bordreuil et al., 2003) for a rigid plastic matrix material in the case of small void volume fraction with no interaction between cavities. The basis of this approach is the representation theory developed by Wang (1970) and adapted to the anisotropic case by Boehler (1978). These developments follow closely the plastic spin theory discussed by Dafalias (1987). The actual void shape is approximated by an ellipsoid.

The orientation is given by the spin of the frame attached to the void relative to the frame attached to the material

$$\begin{aligned}\mathbf{W}^{\text{ellipsoid}}_{\text{material}} &= \eta_1(\mathbf{D}^{\text{p}}\cdot\mathbf{A}_1 - \mathbf{A}_1\cdot\mathbf{D}^{\text{p}}) + \eta_2(\mathbf{D}^{\text{p}}\cdot\mathbf{A}_2 - \mathbf{A}_2\cdot\mathbf{D}^{\text{p}})\\ &\quad + \eta_3(\mathbf{A}_2\cdot\mathbf{D}^{\text{p}}\cdot\mathbf{A}_1 - \mathbf{A}_1\cdot\mathbf{D}^{\text{p}}\cdot\mathbf{A}_2),\end{aligned} \tag{6}$$

where $\mathbf{D}^{\text{p}}$ is the plastic strain rate tensor, $\mathbf{A}_i = \mathbf{n}_i \otimes \mathbf{n}_i$ is a tensor representing the orientation of the ellipsoid eigen direction. Here, the radii of the void are assumed constant during the infinitesimal orientation change. The expressions η_i are functions of the shape ratio ($\lambda = r_1/r_2$) of the ellipsoid. These functions control the reorientation of the frame attached to the ellipsoidal void. The following empirical expressions have been proposed in Bordreuil et al. (2003):

$$\eta_i = f(\lambda_i) = \frac{0.88}{|\ln(\lambda_i)|^{0.58}}. \tag{7}$$

The functions were identified by fitting finite element computation of a 3D cell with a tilted ellipsoidal void and different aspect ratios (λ ranging from 1.25 to 3). The chosen functions give an infinite rotation for a spherical void. This means that this kind of void rotates immediately in the direction of the loading. This feature is also introduced in the model developed in Kailasam and Ponte-Castañeda (1998).

The equation of the radii evolution has to be modified with the orientation changes. Previous developments (Bordreuil, 2002) have shown that the direction of the radii evolution can be obtained by replacing n_{ii} in Eq. (2) by

$$\bar{n}_{ii} = ((\mathbf{Q}^{\text{ellipsoid}}_{\text{material}})^{\text{T}}\cdot\mathbf{n}\cdot\mathbf{Q}^{\text{ellipsoid}}_{\text{material}}) : \delta_{ii}, \tag{8}$$

where $\mathbf{Q}^{\text{ellipsoid}}_{\text{material}}$ is a tensor representing the orientation of the frame attached to the ellipsoid compared to the frame attached to the material. $\mathbf{n}$ is defined before. In any kind of nonlinear analysis, the actual stress has to be calculated in the material frame. So, the previous equation was proposed to transform the components from

the material frame to the ellipsoidal void frame, $\bar{\mathbf{n}} : \delta_{ii}$ is the projection of the tensor on the eigen directions of the void.

4.4. Nucleation/interface debonding

As described so far in the presented model, the interaction between matrix and inclusion is a unilateral contact with an initially debonded interface. The void is then assumed to be initially present and grow as soon as the strain heterogeneity arises. No nucleation step in the damage process is considered. Actually, nucleation is related to interface properties between inclusion and matrix. In reality, physical and chemical bonding as well as thermal fretting induce a non-negligible interface strength between the matrix and the particles. In two previously detailed studies of the damage process of this kind of material (Babout et al., 2001, 2004), nucleation thresholds have been observed for each different inclusion. Particles started to be debonded at different values of the plastic strain. This phenomenon appears also evident in Fig. 2 of the present paper. The fraction of debonded particles continuously increases with the applied strain during a tensile test. This irregularity in the initiation threshold has to be introduced in a physically based damage model because the nucleation threshold automatically delays the onset of growth and then modifies the final amount of void in the material.

Chu and Needleman (1980) introduced the nucleation in an incremental way by adding to the void growth rate $\dot{f}_{\mathrm{G}}$ a contribution of the nucleation $\dot{f}_{\mathrm{N}}$. The void growth rate is virtually increased with the deformation. Our approach is different. The soft metal matrix contains a population of particles with different sizes (see Fig. 2). In the initial RT model, as initially in the modified one used in the present work, the actual population of particles is represented by a single equivalent particle assumed to be able to describe some common behaviour of the different inclusions in the material. It would be more realistic to account for the fact that the material contains a population of inclusions. In the case of no nucleation, Eq. (2) gives the value of the macroscopic growth rate $\dot{r}_i^{\text{no nucl}}$ if all the particles of this population are growing from the very start of the straining. Actually, only a portion ω of the total population of inclusions contributes to this growing rate. Hence, a function ω is introduced for a weighting of $\dot{r}_i^{\text{no nucl}}$. ω comes from the experimental observation of the fraction of damaged particles as the one shown in Fig. 5. It ranges from 0 (no nucleation and then no damage) to 1 (nucleation on every particle). ω is a function of the macroscopic cumulated plastic strain in tension $\bar{\varepsilon}^{\mathrm{p}}$. The expression of $\dot{r}_i^{\text{nucl}}$, the modified void growth rate including nucleation is

$$\dot{r}_i^{\text{nucl}} = \dot{r}_i^{\text{no nucl}}\, \omega(\bar{\varepsilon}_{ii}^{\mathrm{p}}), \tag{9}$$

where $\bar{\varepsilon}_{ii}^{\mathrm{p}} = \boldsymbol{\varepsilon}^{\mathrm{p}} : \delta_{ii}$ is slightly different from the classical cumulated plastic strain as some irreversible process has to be introduced when compressive loading takes place (see Eq. (12) for details).

The criterion is intrinsically isotropic i.e. it has the same critical value for any loading direction. The mechanical loading will, however, induce a difference of the predicted nucleation process along different directions due to the presence of the inclusion. Chu and Needleman (1980) chose a normal distribution of the debonding

strain at the different sites. The quadrature of this function exhibits an "S" shape as a function of strain. The mathematical expression of the weight function—to be compared with an integrated normal distribution of the nucleation with strain—is chosen in the present work as an extremely simple linear relation, more suitable to describe the evolution shown in Fig. 5

$$\omega(\bar{\varepsilon}^{\mathrm{p}}_{ii}) = 0 \quad \text{if } \bar{\varepsilon}^{\mathrm{p}}_{ii} \leqslant \bar{\varepsilon}^{\mathrm{p}}_{0}, \tag{10}$$

$$\omega(\bar{\varepsilon}^{\mathrm{p}}_{ii}) = \alpha\bar{\varepsilon}^{\mathrm{p}}_{ii} + \beta \quad \text{if } \bar{\varepsilon}^{\mathrm{p}}_{ii} > \bar{\varepsilon}^{\mathrm{p}}_{0}. \tag{11}$$

This evolution takes into account the experimental progressive nucleation of the different sites. Again, nucleation is closely related to interface properties which vary from alloy to alloy. As a consequence, the strain criterion proposed here has to be identified in each case with key experiments. No intrinsic solution exists for this kind of nucleation model in the case of inclusion/matrix debonding. The recent work of Babout et al. (2004) has shown that this is a complex issue.

4.5. Model implementation

The model is numerically integrated with a Euler forward scheme by increasing incrementally the macroscopic plastic strain. The increment size used is sufficiently small to assume a linear evolution of the material parameters during the total increment step. It is a two-level algorithm with:

- computation of the radii, integration of Eq. (2) modified with Eq. (8) fulfilling the unilateral condition given by Eq. (4).
- computation for fixed radii of the orientation, Eq. (6) being integrated using the results of (7). The relative rotation between the material and the working frame does not exist in the simple uniaxial straining (tension and compression).

The void volume fraction and triaxiality is assumed to be sufficiently small to allow us to neglect the induced modification of the plastic flow.

In order to compute the radii, the tensile plastic strain has to be evaluated first. This is quantified by a so-called "cumulated plastic strain" in the matrix close to the interface relative to the defect frame as suggested in Gilormini et al. (1993). This variable is calculated by integrating the strain rate expressed in the void's frame

$$\varepsilon^{\mathrm{p}}_{ii_{n+1}} = \varepsilon^{\mathrm{p}}_{ii_n} + \sup((\mathbf{Q})^{\mathrm{void}}_{\mathrm{material}} \cdot \Delta\boldsymbol{\varepsilon} \cdot \mathbf{Q}^{\mathrm{material}}_{\mathrm{defect}})_{ii}, 0). \tag{12}$$

4.6. Summary

The model developed has some drawbacks and holds for:

- low void volume fraction of inclusions (no void interaction),
- low triaxiality ratio,
- spherical inclusions damaging by interface decohesion.

Only nucleation and growth are described (coalescence is not considered). It is an uncoupled approach as the void growth does not modify the plastic flow. A coupled approach could be developed on a thermodynamical base like the Rousselier model (1981). Such an improvement is out of the scope of the present study. Besides, it was checked that the effect of the porosity change on the global behaviour is negligible when the void fraction is small.

The proposed model contains several enhancements to the RT model and is closer to the actual phenomena, especially in the case of the model material reinforced with spheres used in the present study. It deals with some new aspects such as the orientation change of the defects during straining and strain hardening of the matrix material.

5. Experimental validation of the model

The comparison between the model and the measurements performed thanks to the images obtained using X-ray tomography experiments on the model material is presented in this section. This validation is performed at two different scales. At a global scale, the amount of porosity measured and shown in Fig. 5 is compared with the result of the damage model including the nucleation step. At a local scale, the multi-path experiment is then used to validate the model for the orientation changes of the cavities.

5.1. Validation at the global scale

Fig. 6 shows the result of the calculation of the total fraction of void f and its evolution with the plastic strain during a tensile experiment. The damage prediction is calculated for four different conditions:

- Perfectly plastic matrix with no nucleation threshold, Huang's solution.
- Perfectly plastic matrix with no nucleation threshold, RT's approximation.
- Perfectly plastic matrix with the nucleation following the experimental evolution measured by X-ray tomography (Fig. 5).
- The matrix material exhibits a linear strain hardening experimentally identified on the un-reinforced material (see Table 1) and nucleation follows the experimental evolution measured by X-ray tomography (Fig. 5).

The figure also shows the total void fraction measured experimentally and already plotted in Fig. 5 for comparison with the three different modelling predictions. The first two modelling hypotheses (i.e. no hardening of the matrix and no nucleation threshold) lead to an overestimation of the experimental evolution of damage in terms of void fraction in the material.

As expected, the Huang's solution is above the RT one. The agreement obtained with the assumptions closest to the actual phenomenon even if we use RT as an approximation is remarkable. It should be noted that a calculation with Huang's

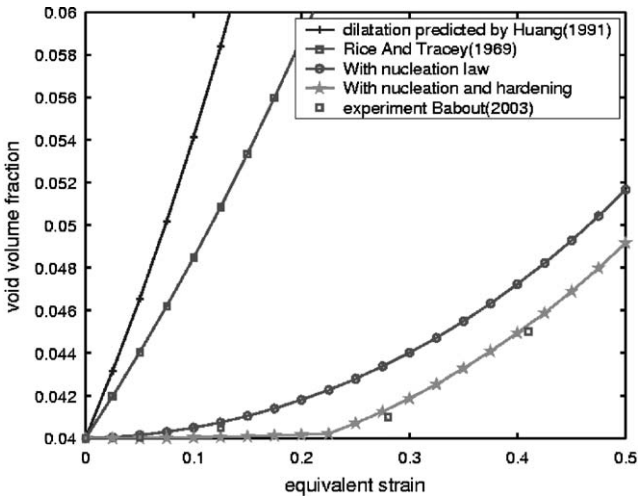

Fig. 6. Predictions of the total void fraction. The computation is performed with different modelling hypotheses: Huang's approximation, RT approximation, with or without hardening of the matrix and with or without nucleation threshold. The experimental void volume fraction measured by X-ray tomography is also shown in the figure.

solution accounting for hardening would certainly also give a reasonable agreement with the experimental data. It is worthwhile to notice that no adjustable parameters are used in the present approach. Every parameter is experimentally measured and only an accurate mechanical formulation of the physical processes involved in the problem can explain the good agreement reached. To our knowledge, this is the first time that these conclusions can be drawn in such good conditions of comparison between modelling and experiments. This also validates the new and simple procedure proposed in this paper for the introduction of the nucleation threshold. The values of the parameters α and β necessary to represent the experimental evolution of the fraction of debonded particles were, respectively, 1.65 and 1.

5.2. *Validation at the local scale*

As mentioned earlier, the validation of the void rotation is of great scientific significance. This improvement in the description of the microstructural phenomena included in the present model could lead to some important findings in modelling of metal forming. An attempt to perform a global validation of the void orientation change using the multi-path experiment described in Section 2.3 has been unsuccessful because the number of cavities formed during the first deformation step was too small to allow a statistical validity of the results. The measurements of the orientation of the entire population of cavities was very difficult because this orientation depends on the aspect ratio of each void. The orientation change of voids which have grown extensively during the tensile loading path is obviously different from the smaller ones. So, the validation of the rotation description of the damage

model was made on the basis of the local observation shown in Fig. 3. As mentioned in a previous section, only one cavity was sufficiently opened after tension to remain measurable after compression. It can be argued that this weakens the statistical validity of our comparison. The physical explanation for this experimental observation (i.e. pores exist after tension but are closed by the compression loading) is that there is no nucleation stage for the process of closing the opened pores in compression. It is then quite natural that the weakly opened pores are quickly closed in compression. The model used is actually able to predict this phenomenon. This observation is then in a certain way a validation of the physical approach used in the present study. This observation clearly indicates that the compression step was a bit too strong in the experiment. This would have been quite difficult to anticipate during the experiment because tomography has the drawback that the data cannot be analysed before they are reconstructed. This implies that the information is only available once the experiment is finished. Future works will probably allow another experiment to be carried out using compression at small and increasing strain increments with intermediate tomographic analysis. This would allow a more dynamic study of the closing process and a more statistical and accurate comparison between experiment and rotation models to be done.

For the case of the only observation we have, the multi-path experiment is compared with a two-step numerical integration of the variables during:

- a tension up to a strain of 0.5 followed by
- a subsequent compression up to a strain of 0.5 at 45° of the tensile direction.

For the sake of simplicity, the matrix material was assumed to be rigid plastic. During the tensile test, the void radii were assumed to first increase only in one direction and then to decrease in compression, with a rotation of the void. These two hypotheses are confirmed by the experimental observations shown in Section 2.

The actual tensile loading path of the experiment could not be reproduced exactly unlike in the previous validation, because each of the three loading steps was followed by an annealing treatment that modifies the hardening behaviour of the matrix material. Furthermore, the values of the parameters α and β previously used for the physical description of the nucleation process were fitting the progressive damage of a population of particles. They are then not suited for the nucleation step around a single inclusion, situation which is of main interest in the present section. The parameters (α and β) were identified on the tensile loading path in such a way as to obtain close values between the predicted void radius and the experimental one after tension. α and β were chosen to reproduce the step function from 0 to 1 of an instantaneous debonding which is a good approximation of the function ω in the local nucleation case. The corresponding values were 40 for α and -4 for β. Once the tensile loading path was modelled and fitted, the compression could be predicted, with a value of 1 for ω for the first radius and calculating the nucleation criterion for the other radii.

The results of the computation of the dimension and the orientation of the observed void are shown in Figs. 7 and 8, respectively. The same nucleation criterion

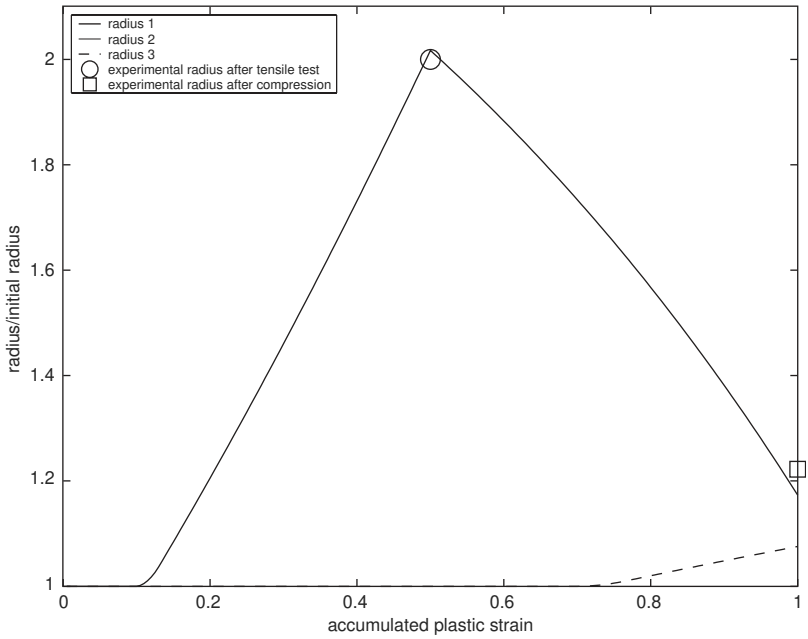

Fig. 7. Comparison between experimental (see Fig. 3) and predicted cavity radii. The calculation is performed in the three main directions of the inclusion. The only measurable experimental radius is in direction 1.

was used for both loading paths. The prediction was performed for the three void radii. The experimental values of the dimension and orientation of the more elongated radius are also shown in the figure. The decrease experimentally measured during the compression path of the radius is reasonably well reproduced by the model. With the nucleation criterion identified on the evolution of the first radius in tension, the model predicts that nucleation occurs for the second and the third radii during the compression loading path. The predicted values of the radii changes during compression are so small that they were not clearly observed in the experimental images. The correlation for the orientation change is reasonable; this good agreement validates the present damage model. The quality of the comparisons has to be outlined as the experimental conditions met closely for the first time the assumptions of the damage model.

The evolution of the equivalent tensile plastic strain (which is subsequently used to calculate the ω function) calculated in the three different directions of the system during the previous fitting procedure is given in Fig. 9 as a function of the accumulated plastic strain applied in tension (0–0.5) and then in compression (0.5–1). The three values (one in each direction) of the ω function subsequently calculated is represented versus the accumulated plastic strain in Fig. 10. The macroscopic strain rate is assumed to be unaffected by the presence of the defect. The strain rate is considered as constant in amplitude and direction in the Eulerian and the material frames; no rotation of the cell is considered in this test. The defect

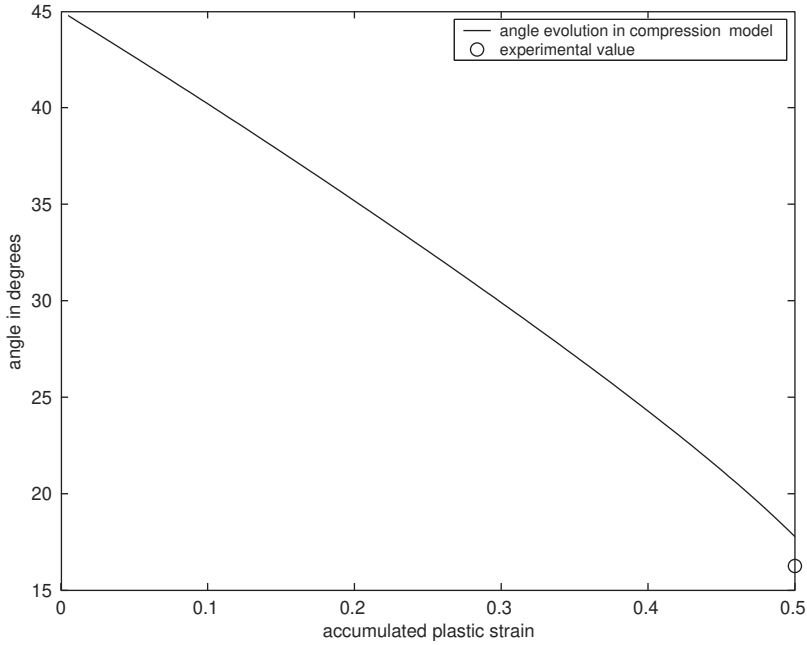

Fig. 8. Comparison of the experimental (see Fig. 3) and predicted cavity orientation.

rotation under plastic straining should affect the cumulative plastic strain even for fixed plastic strain rate. Finite element simulations of forming processes with and without the orientation formulation in the damage model showed that the local phenomenon has no influence on the global behaviour in the case of low void volume fraction.

The accumulated tensile plastic strain controls first the nucleation and then the ω function which in turn affects the growth rate. Once ω has reached its maximum value of 1 for the main radius, it keeps this value as the compression does not completely close the void. The change of these two parameters is very weak for the third radius which is perpendicular to the plane of the extracted tomographic slices shown in Fig. 3. However, the parameters for the second radius show some growth but lower than the detection threshold of the tomography technique.

6. Conclusion

Special model materials have been produced for the present original study with a controlled simple microstructure. A low volume fraction of hard spherical inclusions was mixed in the matrix to nucleate voids. The damage process was studied in the bulk of the materials by the X-ray microtomography technique. The observations were made during an in situ tensile test and also during an ex situ multi-path cold deformation experiment consisting of a tensile path followed by a compression at 45°

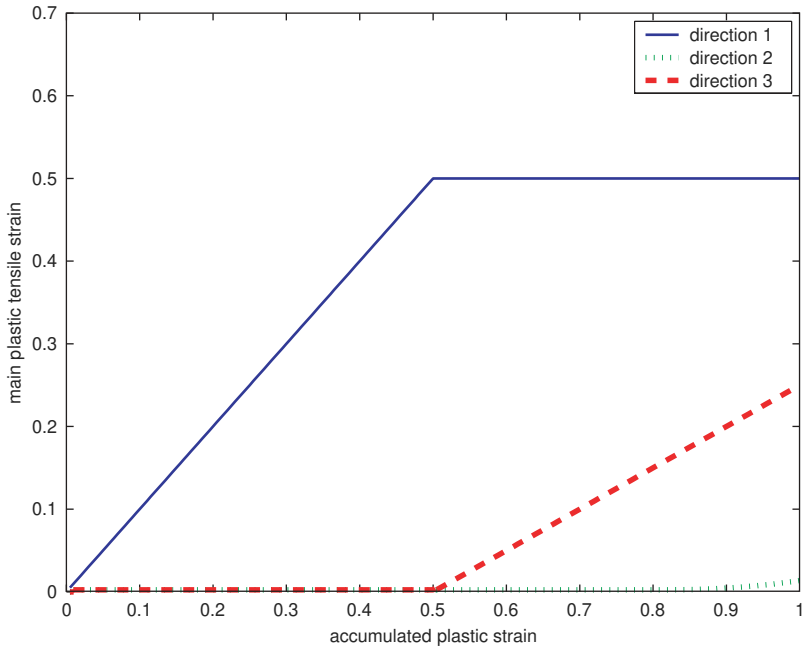

Fig. 9. Evolution of the equivalent tensile plastic strain in the frame of the ellipsoid versus the applied plastic strain during the multi-path loading—0–0.5 = tension loading; 0.5–1 = compression loading. This parameter can be calculated in the three main directions around the inclusion and is subsequently used to calculate the amount of damage initiation (see Fig. 10).

of the tensile direction. These observations were used to validate a physical extension of the RT model for void growth that takes into account:

- the presence of an inclusion in the growing void,
- a plastic hardening behaviour of the matrix,
- the rotation of the voids during multi-step loading.

For the present work, the nucleation step of the damage process was introduced in the existing model. This important improvement considers a void population with a scattered nucleation threshold modelled by a weighting function ω of the mean void growth rate. This weighting function ω is identified experimentally by the measurement of the fraction of damaged particles versus the equivalent plastic strain.

This simple modification leads to a better agreement between the measurements and the predictions of the void fraction. The validation step showed that the plastic strain hardening and the nucleation threshold have to be introduced in any damage model for better predictions of the global amount of damage. At the local scale, the multi-path experiment is a first validation of the void orientation change proposed in

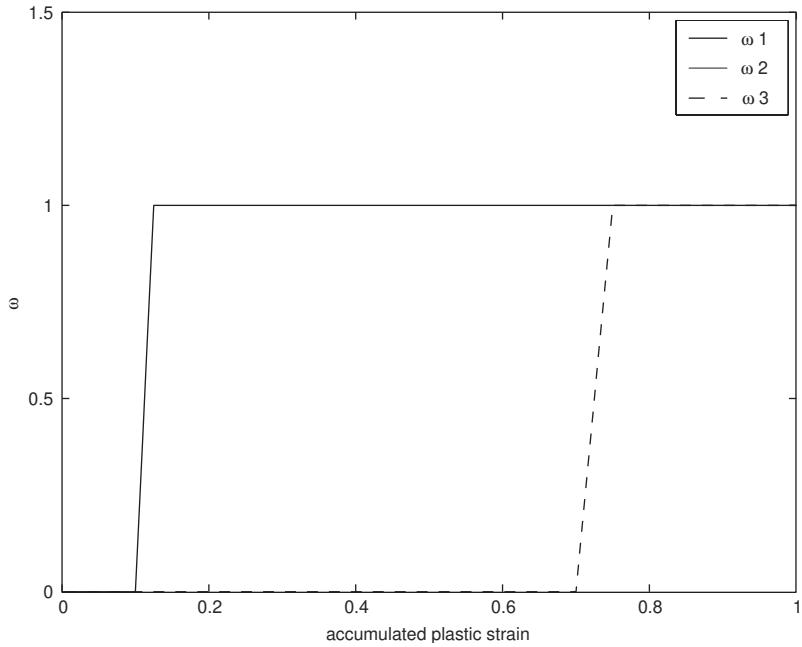

Fig. 10. Evolution of the weight function ω versus the applied plastic strain during the multi-path loading—0–0.5 = tension loading; 0.5–1 = compression loading. This parameter can be calculated in the three main directions around the inclusion.

the present work. This damage model will be particularly fruitfull to improve the modelling of multi-step loadings encountered, for example, in metal forming process.

Acknowledgements

The authors wish to thank the staff of the ID 19 beam line at ESRF (P. Cloetens and E. Pereiro) for their support during tomography experiments and Jose Ferreira at INSA for interfacing the compression stage.

References

<http://www.esrf.fr/expfacilities/id19/homepage/id19homepage.html>, web site, 2000.
<http://www.zirpro.com>, web site, 2000.
Babout, L., Maire, E., Buffière, J.Y., Fougères, R., 2001. Characterization by X-ray computed tomography of decohesion, porosity growth and coalescence in model metal matrix composites. Acta Materiala 49, 2055–2063.
Babout, L., Maire, E., Fougères, R., 2004. Damage initiation in model metallic materials: X-ray tomography and modelling. Acta Materiala 52, 2475–2487.
Benzerga, A., Besson, J., 2001. Plastic potential for plastic anisotropic porous solids. Eur. J. Mech. A/Solids 20, 397–434.

Beremin, F.M., 1981. Cavity formation from inclusions in ductile fracture of A508 steel. Metall. Trans. 12A, 723–731.

Bilby, B.A., Kolbuszewski, M.L., 1977. The finite deformation of an inhomogeneity in two-dimensional slow viscous incompressible flow. Proc. R. Soc. London A 355, 335–353.

Boehler, J.-P., 1978. Lois de comportement anisotrope des milieux continus. J. Mécanique 17 (2), 153–190.

Bordreuil, C., 2002. Un modèle numérique d'endommagement orthotrope pour des transformations finies. Ph.D. Thesis, Institut National des Sciences Appliquées, L.M.So.

Bordreuil, C., Boyer, J.-C., Sallé, E., 2003. On modelling orientations changes in rigid plastic matrix. Model. Simul. Mater. Sci. Eng. 69, 119–138.

Bordreuil, C., Sallé, E., Boyer, J.-C., 2004. A specific orthotropic damage model at finite strains. J. Mater. Proc. Technol. 69, 119–138.

Budiansky, B., Hutchinson, J.W., Slutsky, D.R., 1982. Void growth and collapse in viscous solids, Mechanics of Solids, Pergamon, New York, pp. 13–46.

Buffière, J.Y., Maire, E., Cloetens, P., Lormand, G., Fougères, G., 1999. Characterization of internal damage in a MMCp using X-ray synchrotron phase contrast microtomography. Acta Materiala 47 (5), 1613–1625.

Chu, C.C., Needleman, A., 1980. Void nucleation in biaxially stretched sheets. J. Eng. Mater. Technol. 102, 249–256.

Dafalias, Y., 1987. Issues on the constitutive formulation at large elastoplastic deformations, part 1: kinematics. Acta Mechanica 69, 119–138.

Dierickx, P., Verdu, C., Reynaud, A., Fougères, R., 1996. A study of physico-chemical mechanisms responsible for damage of heat treated and as-cast ferritic spheroïdal graphite cast irons. Scripta Metall. 34, 261–268.

Fleck, N., Hutchinson, J.W., 1986. Void growth in shear. Proc. R. Soc. London 41–54.

Gilormini, P., Roudier, P., Rougée, P., 1993. Les déformations cumulées tensorielles. C. R. Acad. Sci. Paris 316 (II), 1499–1504.

Gologanu, M., Leblond, J.B., Devaux, J., 1994. Approximate models for ductile metals containing nonspherical voids-case of axisymmetric oblate ellipsoidal cavities. J. Eng. Mater. Technol. 290–297.

Gurson, A.L., 1977. Continuum theory of ductile rupture by void nucleation and growth and flow rules for porous ductile media. J. Eng. Mater. Technol. 2–15.

Huang, Y., 1991. Accurate dilatation rates for spherical voids in triaxial stress fields. J. Appl. Mech. 58, 1084–1085.

Humphreys, F.J., 1989. In-situ sem studies of the fracture of aluminium particulate composites. In: Proceedings of EMAG MICRO 89. IOP Publishing Ltd., London, pp. 465–468.

Kailasam, M., Ponte-Castañeda, P., 1998. A general theory for linear and non-linear particulate media with microstructure evolution. J. Mech. Phys. Solids 46, 427–465.

Leblond, J.-B., Perrin, G., Devaux, J., 1995. An improved gurson type model for hardenable ductile metals. Eur. J. Mech./A 14, 499–527.

Lee, B.J., Mear, M.E., 1992. Axisymmetric deformation of power law solids containing a dilute concentration of aligned spheroidal voids. J. Mech. Phys. Solids 1805–1836.

Llorca, J., Martin, A., Ruiz, J., Elices, M., 1993. Particulate fracture during deformation of a spray formed metal–matrix composite. Metall. Trans. 24A, 1575–1588.

Maire, E., Buffière, J.Y., Salvo, L., Blandin, J.J., Ludwig, W., Letang, J.M., 2001. On the application of X-ray microtomography in the field of materials science. Adv. Eng. Mater. 3 (8), 539–546.

Manoharan, M., Lewandowski, J.J., 1989. In situ deformation studies of an aluminium metal–matrix composite in a scanning electron microscope. Scripta Metall. 23, 1801–1804.

Pardoen, T., Hutchinson, J.W., 2000. An extended model for void growth and coalescence. J. Mech. Phys. Solids 48, 2467–2512.

Poza, P., Llorca, J., 1996. Fracture toughness and fracture mechanisms of Al–Al_2O_3 composites at cryogenic and elevated temperatures. Mater. Sci. Eng. 206A (2), 183–193.

Rice, J.R., Tracey, D.M., 1969. On the enlargement of voids in triaxial stress fields. J. Mech. Phys. Solids 201–217.

Rousselier, G., 1981. Finite deformation constitutive relations including ductile fracture damage. In: Nemat-Nasser (Ed.), Three Dimensional Constitutive Relations and Ductile Fracture. Pergamon Press, New York, pp. 311–315.

Sarkar, J., Kutty, T.R.G., Konlon, K.T., Wilkinson, D.S., Embury, J.D., Lloyd, D.J., 2001. Tensile and bending properties of aa5754 aluminum alloys. Mater. Sci. Eng. A 316, 52–59.

Semiatin, S.L., Seetharaman, V., Ghosh, A.K., Shell, E.B., Simon, M.P., Fagin, P.N., 1998. Cavitation during hot tension testing of ti-6al-4v. Mater. Sci. Eng. A 256, 91–110.

Thomason, P.F., 1988. Ductile Fracture of Metals. Pergamon Press, New York.

Tvergaard, V., Needleman, A., 1984. Analysis of cup cone fracture in round tensile test bar. Acta Metall. 157–169.

Verhaege, B., Louchet, F., Bréchet, Y., Massoud, J.P., 1997. Damage and rupture mechanisms in an austenoferritic duplex steel. Acta Materiala 45, 1811–1819.

Wang, C.C., 1970. New theorem for isotropic function part 1 and part 2. Arch. Ration. Mech. An. 36, 166–223.